Supporting Information – Pinching a glass reveals key properties of its soft spots

Corrado Rainone,[1] Eran Bouchbinder,[2] and Edan Lerner[1]

[1] *Institute for Theoretical Physics, University of Amsterdam, Science Park 904, Amsterdam, Netherlands*

[2] *Chemical and Biological Physics Department, Weizmann Institute of Science, Rehovot 7610001, Israel*

In this Supporting Information we provide information about (*i*) how the bulk-average frequency of the response to a local pinch of the glass, denoted ω_g in the manuscript, was calculated, (*ii*) how the modes in Fig. 1 of the main text were calculated, and their size estimated, and (*iii*) how we estimated the crossover length $\xi_{\rm co}$ and the QLMs core size $\xi_{\rm QLM}$, both appearing in Fig. 6 of the main text.

We recall that lengths are expressed in terms of $a_0 \equiv V/N$ where V is the system's volume, and N denotes the number of particles. All particles share the same mass m, which we set as our microscopic unit of mass. Frequencies are expressed in terms of c_∞/a_0, where $c_\infty \equiv \sqrt{G_\infty/\rho}$ is the high-T_p shear wave-speed, with G_∞ denoting the high-T_p plateau of sample-to-sample mean athermal shear modulus of inherent states (see inset of Fig. 3a of main text), and $\rho \equiv mN/V$ denotes the mass density. Temperatures are expressed in terms of the crossover temperature $T_{\rm onset}$, above which the sample-to-sample mean athermal shear modulus saturates to a high-temperature plateau, as seen in Fig. 4 of the main text, and in [1]. In our system we find $G_\infty a_0^3/k_B T_{\rm onset} \approx 17$, with k_B denoting the Boltzmann constant.

S-1. The calculation of $\omega_g(T_p)$

Following [2], we define a local dipolar force as

$$\boldsymbol{d}_k^{(ij)} \equiv \frac{\partial \varphi_{ij}}{\partial \boldsymbol{x}_k} \,, \tag{S1}$$

where Roman indices denote particle indices, φ_{ij} is the radially-symmetric pairwise potential between the $i^{\rm th}$ and $j^{\rm th}$ particles, and $\boldsymbol{x}_k$ denotes the $\hat{d}$-dimensional coordinate vector of the $k^{\rm th}$ particle. The linear displacement response to this force dipole reads

$$\boldsymbol{u}_k^{(ij)} = \boldsymbol{\mathcal{H}}^{-1}_{k\ell} \cdot \boldsymbol{d}_\ell^{(ij)} \,, \tag{S2}$$

where repeated indices are understood to be summed over, and

$$\boldsymbol{\mathcal{H}}_{k\ell} \equiv \frac{\partial^2 U}{\partial \boldsymbol{x}_k \partial \boldsymbol{x}_\ell} \tag{S3}$$

is the Hessian of the potential energy $U \equiv \sum_{i<j} \varphi_{ij}$. The frequency associated with the response $\boldsymbol{u}$ is given by

$$\omega_g^{(ij)} \equiv \frac{1}{\sqrt{m}} \left(\frac{\boldsymbol{u}_k^{(ij)} \cdot \boldsymbol{\mathcal{H}}_{k\ell} \cdot \boldsymbol{u}_\ell^{(ij)}}{\boldsymbol{u}_k^{(ij)} \cdot \boldsymbol{u}_k^{(ij)}} \right)^{1/2} \,, \tag{S4}$$

where m denotes the microscopic units of mass.

We next define the conditional average

$$\omega_g \equiv \langle \omega_g^{(ij)} \rangle_{f_{ij}/(pa_0^2)<10^{-2}} \,, \tag{S5}$$

where p is the glass pressure (recall that in our computer glass particles interact via a purely repulsive pairwise interaction), and the triangular brackets denote an average taken over all interacting pairs i,j for which the dimensionless pairwise force $f_{ij}/(pa_0^2) < 10^{-2}$.

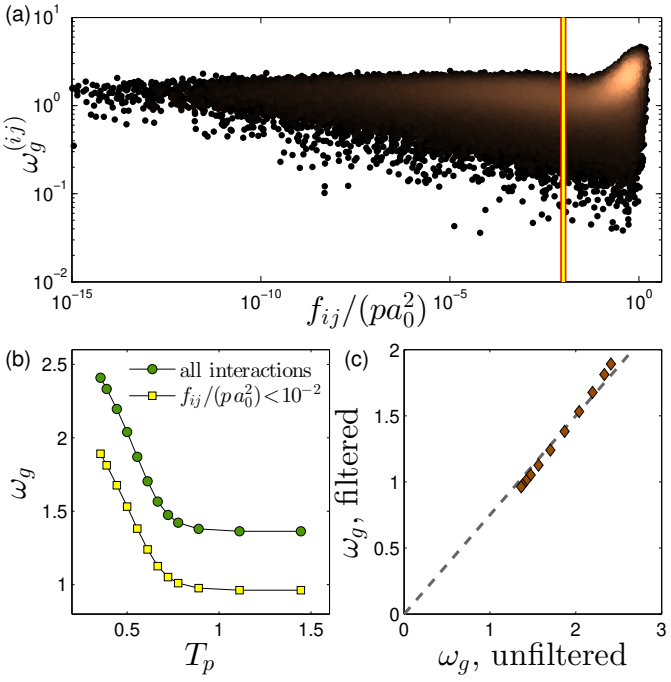

FIG. S1. (a) Scatter plot of $\omega_g^{(ij)}$ vs. the dimensionless pairwise force $f_{ij}/(pa_0^2)$, calculated in an ensemble of glassy solids quenched from $T_p = 5/9$. Results for other parent temperatures have similar forms. At strong forces the stiffnesses associated with responses to local pinches are substantially higher compared to those associated with weak forces. We find a saturation of the statistics of $\omega_g^{(ij)}$ at $f_{ij}/(pa_0^2) \lesssim 10^{-2}$, marked by the vertical line. (b) & (c) Comparison between the mean frequencies ω_g calculated with and without filtering by the pairwise forces; the two means differ by $\approx 40\%$ consistently throughout the sampled temperature range.

The reason we chose to only consider weak forces in the estimation of ω_g can be understood by scatter-plotting $\omega_g^{(ij)}$ vs. $f_{ij}/(pa_0^2)$, as seen in Fig. S1a. We can clearly see that two families of frequencies are generated by pinching pairs between which strong or weak forces are found. In particular, strongly-interacting pairs tend to

generate much stiffer responses (note the logarithmic y-axis). Since these responses are supposed to represent soft, quasilocalized modes, we opt for filtering the responses according to the dimensionless forces $f_{ij}/(pa_0^2)$. Below the chosen threshold $f_{ij}/(pa_0^2) < 10^{-2}$, that can be clearly read off the scatter plot Fig. S1 (vertical yellow line), the statistics of $\omega_g^{(ij)}$ appears to saturate.

In Fig. S1b,c we examine the effect of filtering interactions by their force on the T_p dependence of ω_g. We see that the relative variation of the two mean frequencies is very similar throughout the sampled parent-temperature range.

S-2. Calculation of soft modes in 2D

In this Section we describe how the modes shown in Fig. 1 of the main text were calculated. A detailed description of this calculation will be presented elsewhere [3], and see also [4]; here the main points are summarized.

We employed the two-dimensional version of the same computer glass model used for our study; details about the model can be found in [5]. Ensembles of glassy samples were quenched from equilibrium parent temperatures of $T_p = 7/9$ (expressed in terms of the onset temperature $T_{\rm onset}$ as described above) and $T_p = 17/90$. We followed the framework put forward in [4, 6], and calculated solutions $\boldsymbol{\pi}$ to the equation

$$\boldsymbol{\mathcal{H}}\cdot\boldsymbol{\pi} = \frac{\boldsymbol{\pi}\cdot\boldsymbol{\mathcal{H}}\cdot\boldsymbol{\pi}}{\frac{\partial^4 U}{\partial\boldsymbol{x}\partial\boldsymbol{x}\partial\boldsymbol{x}\partial\boldsymbol{x}} :: \boldsymbol{\pi}\boldsymbol{\pi}\boldsymbol{\pi}\boldsymbol{\pi}} \frac{\partial^4 U}{\partial\boldsymbol{x}\partial\boldsymbol{x}\partial\boldsymbol{x}\partial\boldsymbol{x}} :\cdot \boldsymbol{\pi}\boldsymbol{\pi}\boldsymbol{\pi}\,, \quad \text{(S6)}$$

where triple and quadruple contractions are denoted as $:\cdot$ and $::$, respectively, and particle indices were suppressed for simplicity. Solutions $\boldsymbol{\pi}$ to Eq. (S6) were coined 'quartic modes' [2, 4]; they represent soft quasilocalized excitations that resemble low-frequency quasilocalized vibrational modes seen below or in between phonon bands [6], i.e. in the absence of hybridizations with phonons. Solutions to Eq. (S6) were calculated by employing a standard nonlinear conjugate gradient minimization algorithm to find local minima of the cost function [6]

$$\mathcal{G}(\boldsymbol{z}) \equiv \frac{(\boldsymbol{z}\cdot\boldsymbol{\mathcal{H}}\cdot\boldsymbol{z})^2}{\frac{\partial^4 U}{\partial\boldsymbol{x}\partial\boldsymbol{x}\partial\boldsymbol{x}\partial\boldsymbol{x}} :: \boldsymbol{z}\boldsymbol{z}\boldsymbol{z}\boldsymbol{z}}\,, \quad \text{(S7)}$$

where $\boldsymbol{z}$ represents a displacement field in the $N\times\bar{d}$ dimensional configuration space of the glass. It is straightforward to show (see further details in [6]) that minima of $\mathcal{G}$ correspond to solutions of Eq. (S6). Initial conditions for the minimization of $\mathcal{G}$ were obtained by calculating the linear displacement response to a dipolar force, as given by Eq. (S2), for every pair of interacting particles in the glass. In Fig. 1 of the main text, we only show modes $\boldsymbol{\pi}$ for which $\omega_{\boldsymbol{\pi}} \equiv \sqrt{\boldsymbol{\pi}\cdot\boldsymbol{\mathcal{H}}\cdot\boldsymbol{\pi}}/\sqrt{m} < \omega_g/3$, where ω_g was calculated as described in the previous Section. The area of the disordered core of each of the calculated modes was estimated as Ne, with e denoting the participation ratio of the modes, defined for a normalized mode $\hat{\boldsymbol{z}}$ as $e = \left(N\sum_i(\hat{\boldsymbol{z}}_i\cdot\hat{\boldsymbol{z}}_i)^2\right)^{-1}$. The participation ratio is a proxy for the degree of localization of a mode; in particular, for a localized mode one expects $e\sim\mathcal{O}(1/N)$, whereas a spatially-extended mode would give $e\sim\mathcal{O}(1)$. In Fig. 1 of the main text, the area of each blob that represents a soft mode is proportional to Ne, and its color represents its frequency $\omega_{\boldsymbol{\pi}}$, with dark (bright) colors representing softer (stiffer) modes.

S-3. Estimation of the crossover length

In this Section we describe how we measured the crossover length $\xi_{\rm co}$ between disorder-dominated responses near a local perturbation, to continuum, Eshelby-like algebraic decays away from a local perturbation. The crossover lengths $\xi_{\rm co}$ extracted from the following analysis are shown in Fig. 6 of the main text.

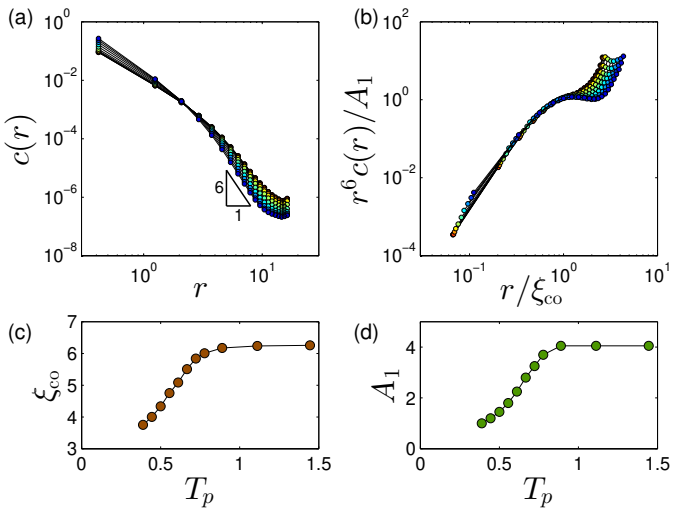

FIG. S2. (a) Decay functions $c(r)$ of the response to local pinches, see text for precise definition. The different curves correspond to measurements performed on glassy samples quenched from $T_p = 13/9, 10/9, 8/9, 7/9, 13/18, 2/3, 11/18, 5/9, 1/2, 4/9, 7/18$, from warm to cold colors. (b) Rescaling $c(r)$ by r^{-6} allows to robustly identify the crossover length $\xi_{\rm co}$ between disorder-dominated to continuum-like scaling. (c) & (d) The crossover lengths $\xi_{\rm co}$ and the factors A_1 used to collapse the curves in panel (b), plotted against the parent temperature T_p.

In order to estimate the crossover length, we follow the measurement scheme of [7]; this amounts to calculating the response to local dipoles via Eq. (S2), still following the dimensionless-force filtering scheme discussed above. The fields are then normalized, namely for every pair ij considered, we calculate $\hat{\boldsymbol{u}}^{(ij)} \equiv \boldsymbol{u}^{(ij)}/|\boldsymbol{u}^{(ij)}|$. Then, for *each* interaction $k\ell \neq ij$, we compute the square of the projection of the normalized response $\hat{\boldsymbol{u}}^{(ij)}$ onto the normalized dipole vector $\hat{\boldsymbol{d}}^{(k\ell)} \equiv \boldsymbol{d}^{(k\ell)}/|\boldsymbol{d}^{(k\ell)}|$, i.e. we cal-

culate

$$C_{ij,k\ell} \equiv \left(\hat{\boldsymbol{u}}^{(ij)} \cdot \hat{\boldsymbol{d}}^{(k\ell)}\right)^2 . \tag{S8}$$

$C_{ij,k\ell}$ generally depends on the distance $r_{ij,k\ell}$ between the interactions ij and $k\ell$, and on their relative orientation.

For each normalized response field $\hat{\boldsymbol{u}}^{(ij)}$, we bin $C_{ij,k\ell}$ — calculated for all pairs $k\ell \neq ij$ — over the distances $r_{ij,k\ell}$, and calculate the *median* of $C_{ij,k\ell}$ over all pairs $k\ell$ located at similar distances r away from the excited dipole $\boldsymbol{d}^{ij}$; the average over the excited dipole ij, and over glassy samples, denoted below by $\langle\bullet\rangle_{ij}$, defines the decay function $c(r)$, namely

$$c(r) \equiv \Big\langle \underset{r_{ij,k\ell}\approx r}{\text{median}_{k\ell}}\big(C_{ij,k\ell}\big)\Big\rangle_{ij} . \tag{S9}$$

The decay functions $c(r)$ are plotted in Fig. S2a. Continuum elasticity would predict that $c(r)\sim r^{-2d}$ [7]. We therefore plot in Fig. S2b the rescaled decay functions $r^6 c(r)/A_1$ against the rescaled distance r/ξ_{co} with $\xi_{\text{co}}(T_p)$ denoting the parent-temperature dependent crossover lengths, chosen to collapse the data, as are the constants $A_1(T_p)$ reported in Fig. S2d. The crossover lengths $\xi_{\text{co}}(T_p)$ are plotted against the parent temperature T_p in Fig. S2c.

S-4. Estimation of QLMs core length

In stable glasses, it becomes difficult to sample many QLMs using a harmonic analysis due to their stiffening and depletion, discussed in length the main text. As a result of these processes, characteristic frequencies of the softest QLMs tend to overlap with the lowest phonon frequencies, leading to hybridizations of phonons and QLMs, and obscuring a clear picture of QLMs properties and statistics, as demonstrated in Fig. S3.

In order to reveal the properties of QLMs for glasses quenched from all parent temperatures, including in stable glasses, we opt for calculating 'quartic modes' as representatives of QLMs, since the former are known to be indifferent to the presence of phonons with comparable frequencies (they show no hybridizations with phonons, as shown in [6] and in the left panel of Fig. S3). At the same time, quartic modes feature frequencies that are in excellent agreement with QLMs' frequencies in the absence of hybridizations [6], as can also be seen in Fig. S3.

We first generated, for each of our glassy samples of $N=8000$ particles, a quartic mode as discussed in length in Sect. S-2. In this case, however, the initial conditions for finding quartic modes were chosen to be the linear displacement responses to the forces that arise due to imposing simple and pure shear [8] in all possible Cartesian planes (i.e. $\hat{x}-\hat{y}, \hat{x}-\hat{z}, \ldots$). Each such linear response is then used as the initial condition for the minimization of the cost function $\mathcal{G}$, c.f. Eq. (S7). An ensemble of

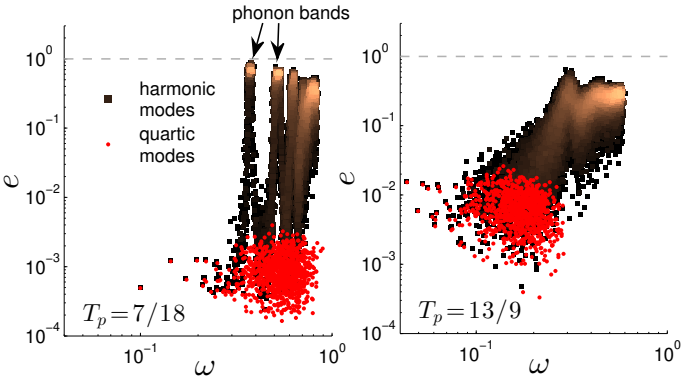

FIG. S3. Scatter plot of the participation ratio e — that quantifies the degree of localization of a mode — vs. frequency, calculated for harmonic (black symbols) and quartic (red symbols) modes in glassy samples of $N = 8000$ particles quenched from $T_p = 7/18$ (left) and $T_p = 13/9$ (right). In the analyzed stable glassy samples ($T_p = 7/18$, left panel) phonons and QLMs dwell at similar frequencies, leading to their hybridizations. Quartic modes appear to be entirely indifferent to the presence of these phonons (see left panel).

QLMs is constructed by only keeping and considering the QLM $\boldsymbol{\pi}$ with the smallest frequency $\omega_{\boldsymbol{\pi}} \equiv \sqrt{\boldsymbol{\pi}\cdot\boldsymbol{\mathcal{H}}\cdot\boldsymbol{\pi}}/\sqrt{m}$ amongst all those calculated *for each individual sample*, leaving us with 1000 soft QLMs per parent temperature T_p.

In order to demonstrate the utility of quartic modes for the assessment of the core size of QLMs, we scatter-plot in Fig. S3 the participation ratio of both harmonic modes (obtained by a partial diagonalization of the Hessian of the potential energy), and quartic modes (obtained as described above). We show that, at the very lowest frequencies, each harmonic mode overlaps with a quartic mode that our calculation produces, demonstrating that our calculation captures well the QLM away from regimes of strong hybridizations with phonons. These data show that harmonic and quartic mode share very similar localization properties and frequencies, as also discussed in length in [6], which motivates employing quartic modes as faithful representitives of QLM.

In order to estimate the linear size of the cores of QLM, each calculated QLM $\boldsymbol{\pi}$ as described above was normalized $\hat{\boldsymbol{\pi}} \equiv \boldsymbol{\pi}/|\boldsymbol{\pi}|$; we then identified the pair ij of interacting particles that maximizes the difference squared $|\hat{\boldsymbol{\pi}}_i - \hat{\boldsymbol{\pi}}_j|^2$, and consider this pair as the center of the QLM's core. We calculated the spatial decay $c(r)$ of QLMs similarly to the procedure explained in the previous Section for analyzing the spatial decay of the response to a local pinch, with the only differences being that here that r represents the distance from the aforementioned pair ij,

$$C_{ij,k\ell} \equiv \left(\hat{\boldsymbol{\pi}} \cdot \hat{\boldsymbol{d}}^{(k\ell)}\right)^2 , \tag{S10}$$

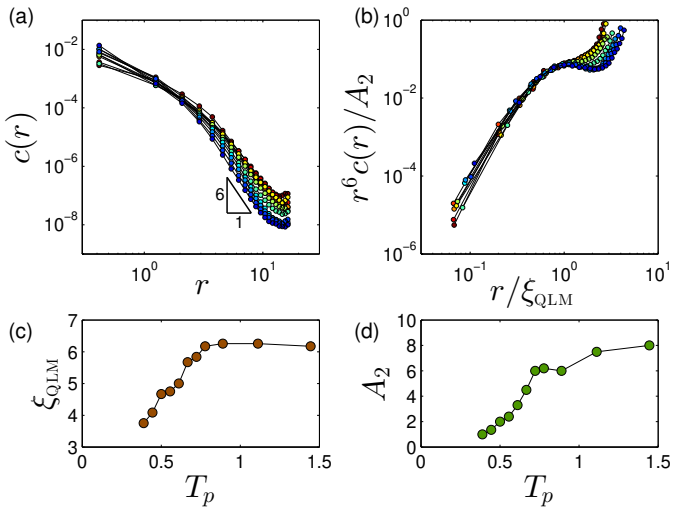

FIG. S4. (a) Decay functions $c(r)$ of QLMs calculated as explained in this SI. The different curves correspond to measurements performed on glassy samples quenched from the same parent temperatures T_p as spelled out in the caption of Fig. S2. (b) Rescaling $c(r)$ by r^{-6} allows to robustly identify the QLMs linear core size $\xi_{\rm QLM}$. (c) & (d) The QLM core length $\xi_{\rm QLM}$ and the factors A_2 used to collapse the curves in panel (b), plotted against the parent temperature T_p.

and

$$c(r) \equiv \left\langle \underset{r_{ij,k\ell}\approx r}{\text{median}_{k\ell}}\big(C_{ij,k\ell}\big)\right\rangle_{\rm QLMs}, \tag{S11}$$

where the average is taken over all calculated QLMs.

The results of this calculation are shown in Fig. S4, see figure caption for further details. The lengths $\xi_{\rm QLM}$ extracted from our analysis are shown in Fig. S4c, and used in Fig. 6 of the main text.

[1] E. Lerner, Mechanical properties of simple computer glasses, J. Non-Cryst. Solids **522**, 119570 (2019).

[2] E. Lerner and E. Bouchbinder, A characteristic energy scale in glasses, J. Chem. Phys. **148**, 214502 (2018).

[3] G. Kapteijns, D. Richard, M. Wesseling, and E. Lerner, Nonlinear quasilocalized excitations in glasses. ii. detection of the complete field of low-energy excitations, *in preparation*.

[4] G. Kapteijns, D. Richard, and E. Lerner, Nonlinear quasilocalized excitations in glasses. i. true representatives of soft spots, arXiv preprint arXiv:1912.10930 (2019).

[5] A. Moriel, G. Kapteijns, C. Rainone, J. Zylberg, E. Lerner, and E. Bouchbinder, Wave attenuation in glasses: Rayleigh and generalized-rayleigh scattering scaling, J. Chem. Phys. **151**, 104503 (2019).

[6] L. Gartner and E. Lerner, Nonlinear modes disentangle glassy and Goldstone modes in structural glasses, SciPost Phys. **1**, 016 (2016).

[7] E. Lerner, E. DeGiuli, G. During, and M. Wyart, Breakdown of continuum elasticity in amorphous solids, Soft Matter **10**, 5085 (2014).

[8] C. E. Maloney and A. Lemaître, Amorphous systems in athermal, quasistatic shear, Phys. Rev. E **74**, 016118 (2006).